**Astronomy & Astrophysics**

# Disentangling the two sub-populations of early Herbig Be stars using VLT/X-shooter spectra

B. Shridharan[1] , B. Mathew[1], R. Arun[2], T. B. Cysil[1], A. Subramaniam[2], P. Manoj[3],
G. Maheswar[2], and T. P. Sudheesh[1]

[1] Department of Physics and Electronics, CHRIST (Deemed to be University), Bangalore 560029, India
e-mail: shridharan.b@res.christuniversity.in
[2] Indian Institute of Astrophysics, Sarjapur Road, Koramangala, Bangalore 560034, India
[3] Tata Institute of Fundamental Research, Homi Bhabha Road, Mumbai 400005, India

**ABSTRACT**

*Context.* Early Herbig Be (HBe) stars are massive, young stars accreting through the boundary layer mechanism. However, given the rapid (<2 Myr) evolution of early Herbig stars to the main-sequence phase, studying the evolution of the circumstellar medium around these stars can be a cumbersome exercise.

*Aims.* In this work, we study the sample of early (B0–B5) HBe stars using the correlation between H$\alpha$ emission strength and near–infrared excess, complemented by the analysis of various emission features in the X-shooter spectra.

*Methods.* We segregate the sample of 37 early HBe stars based on the median values of H$\alpha$ equivalent width (EW) and near–infrared index ($n$(J−H)) distributions. The stars with |H$\alpha$ EW| > 50 Å and $n$(J−H) > −2 are classified as intense HBe stars and stars with |H$\alpha$ EW| < 50 Å and $n$(J−H) < −2 as weak HBe stars. Using the VLT/X–shooter spectra of five intense and eight weak HBe stars, we visually checked for the differences in intensity and profiles of various HI and metallic emission lines commonly observed in Herbig stars.

*Results.* We propose that the intense HBe stars possess an inner disk close to the star (as apparent from the high near-infrared excess) and an active circumstellar environment (as seen from the high H$\alpha$ EW value and presence of emission lines belonging to FeII, CaII, OI, and [OI]). However, for weak HBe stars, the inner disk has cleared, and the circumstellar environment appears more evolved than for intense HBe stars. Furthermore, we compiled a sample of ~58 000 emission-line stars published in *Gaia* DR3 to identify more intense HBe candidates. Further spectroscopic studies of these candidates will help us to understand the evolution of the inner (approximately a few au) disk in early HBe stars.

**Key words.** stars: emission-line, Be – circumstellar matter – methods: data analysis – techniques: spectroscopic

## 1. Introduction

Herbig Ae/Be (HAeBe) stars are pre-main sequence (PMS) stars belonging to A and B spectral types with their mass ranging from 2 to 10 $M_\odot$ (Herbig 1960; Strom 1972). The optical and infrared (IR) spectra of HAeBe stars are known to show emission lines of various allowed and forbidden transitions such as H$\alpha$, H$\beta$, CaII, OI, and [OI] (Hamann & Persson 1992a; Fairlamb et al. 2015). In addition, they show excess flux in the IR wavelengths due to the energy reprocessing by dust grains in the outer disk (Cohen 1980; Hillenbrand et al. 1992; Malfait et al. 1998). The circumstellar medium of HAeBe stars is active with different emission lines arising from the circumstellar disk, accretion columns, and disk winds around them (refer to Brittain et al. 2023 for a recent review on HAeBe stars).

However, in recent years, studies have noted the distinction between various properties of HBe and HAe stars. Since the mass varies drastically between B and A spectral types, the processes occurring in the stellar interiors also differ between HBe and HAe stars. The properties of accretion (Wichittanakom et al. 2020) and variability (Mendigutía et al. 2011b; Villebrun et al. 2019) have been reported to differ between HAe and HBe stars. One of the significant differences between them is the mode of accretion from the circumstellar disk. HAe and late HBe stars are known to accrete through the magnetospheric accretion (MA) paradigm (see Mendigutía 2020 for a review), where the star's magnetosphere truncates the circumstellar disk at a few stellar radii and funnels the material onto the star through the magnetospheric field lines. Due to the absence of a strong magnetic field (Gregory et al. 2012), early HBe stars do not accrete through MA and instead they do so through the boundary layer (BL) mechanism. In BL mode, the Keplerian circumstellar disk almost reaches the stellar surface and material gets transferred onto the star through the interface between the disk and the stellar surface (known as the BL; Lynden-Bell & Pringle 1974).

An interesting HBe star to note in the context of BL accretion is MWC 297, which is a nearby (~400 pc; Bailer-Jones et al. 2021), massive young star of B1.5V spectral type. This HBe star has been extensively studied and is known to be actively accreting from its circumstellar disk. It is known to have strong Balmer emission (|H$\alpha$ equivalent width (EW)| > 200 Å), double-peaked [OI] emission, and double-peaked CO emission, which is suggestive of the presence of a nearly edge-on circumstellar disk (Drew et al. 1997; Zickgraf 2003; Acke et al. 2008; Banzatti et al. 2022). Further, interferometric observations and modelling of MWC 297 did not reveal a cavity or inner gap in the disk (Acke et al. 2008; Kluska et al. 2020). Thus, MWC 297 accretes material through the BL mechanism. Similar direct pieces of

evidence are not available for other early HBe stars. Hence, this demands the study of a large sample of HBe stars, belonging to diverse environments, to evaluate the mode of accretion and to understand the nature of the circumstellar medium.

The motivation for this work was from Shridharan et al. (2023), where they performed HI line analysis of HAeBe stars using the X-shooter spectra. In addition, they studied the statistical presence of higher-order emission lines of HI in HAeBe stars with respect to the stellar parameters and from which they noticed bimodality in higher-order emission lines in the sample of early (B0–B5) HBe stars. Given that the ages (PMS lifetime) of early HBe stars are less than 2 Myr and the fact that they already lost most of their inner circumstellar disk, the analysis of these objects is vital to bridge the stages in intermediate-mass star formation. Using this as a lead, we checked for the differences between the properties of the two populations, which were identified due to the distinction in the presence of higher-order Balmer emission lines. For the present work, we carried out further analysis and found the presence of two populations of early HBe stars (B0–B5) in the H$\alpha$ versus near-infrared (NIR) excess space. Since H$\alpha$ and NIR excess in HAeBe are known to be associated with the inner (approximately a few au) circumstellar medium (Manoj et al. 2006), we suspect a difference in the circumstellar medium of the two populations. Hence, a study of these two groups can help in understanding the evolution of the inner circumstellar disk in stars undergoing BL accretion. From a search in the literature, we found three instances where two populations of HBe stars are reported. Hillenbrand et al. (1992) found that most of the group III stars (with low NIR excess) have B spectral type, and Corcoran & Ray (1998) proposed a class of 'weak-line' HAeBes for stars with no forbidden line emission and |H$\alpha$ EW| <15 Å. Banzatti et al. (2018) observed a dichotomy in the NIR excess of their group I sources. The group I sources either showed high (>25%) or low (<10%) NIR excess. They also found that the strength of NIR excess is correlated with the radius at which CO is detected. The sources with low NIR excess show CO emission at larger radii compared to sources with high NIR excess, which implies that the inner region is depleted in low NIR excess sources. In this work, we report the detection of two populations of early HBe stars and discuss the distinction between their circumstellar medium.

The paper is structured as follows. The dataset used in this work is explained in Sect. 2. The differences in the NIR excess, H$\alpha$, and spectral features between the two populations are described in Sect. 3. We also evaluate a few interesting questions regarding the identification of two sub-populations of early HBe stars in Sect. 4, followed by a summary of this work in Sect. 5.

## 2. Data used for this study

We combined the well-studied HAeBe catalogues of Vioque et al. (2018) and Guzmán-Díaz et al. (2021) to compile a comprehensive set of stellar parameters. From this combined catalogue, we selected 37 HBe stars with spectral type earlier than B5 (as estimated by Guzmán-Díaz et al. 2021) for our analysis. The NIR magnitudes ($J$, $H$, and $K_S$) used in the study are the photometric data from the Two Micron All Sky Survey (2MASS; Skrutskie et al. 2006) and the mid-infrared (MIR) magnitudes ($W1$, $W2$, and $W3$) are taken from the Wide-field Infrared Survey Explorer (WISE; Cutri et al. 2021). Further, the medium-resolution spectra of HBe stars observed with the X-shooter instrument were retrieved from the archive and are used for the present study. X-shooter is an echelle spectrograph mounted at

the UT3 Cassegrain focus of the VLT telescope (Cerro Paranal, Chile), which provides spectra covering a large wavelength range of 3000–25 000 Å, split into three arms and taken simultaneously. The arms are split into the following: the UVB arm from 3000–5600 Å, the VIS arm from 5500–10 200 Å, and the NIR arm from 10 200–24 800 Å. The smallest slits available with widths of 0.5″, 0.4″, and 0.4″ were used to provide the highest possible resolutions of $R$ = 9700, 18 400, and 11 600 for the respective UVB, VIS, and NIR arms. The X-shooter spectra were directly downloaded from the ESO Phase 3 archive. The spectra were corrected for barycentric radial velocity based on the observation date. Furthermore, we made use of the *Gaia* ELS catalogue (Fouesneau et al. 2023) along with their estimated astrophysical parameters to identify new candidates of intense B-type emission stars, as detailed in Appendix A.

## 3. Analysis and results

In this section, we segregate the early HBe stars into two distinct populations based on the observed H$\alpha$ EW and NIR excess seen in the Spectra Energy Distribution (SED) plot. Further, we outline the differences in the spectroscopic features between two populations of early HBe stars.

### 3.1. Bi-modality in infrared excess and H$\alpha$ EW space

Previously, Manoj et al. (2006) had shown the explicit dependence of NIR excess on the observed H$\alpha$ EW, which suggested the presence of an inner hot disk in HAeBe stars. With the advent of *Gaia* (Prusti et al. 2016) and IPHAS (Barentsen et al. 2014) surveys, homogeneous mass accretion rate studies have been performed in recent years for a well-categorised sample of HAeBe stars (Arun et al. 2019; Vioque et al. 2020; Guzmán-Díaz et al. 2021). As explained, several indirect pieces of evidence suggest that the late HBe and HAe stars accrete through magnetospheric columns, whereas the MA paradigm may not have an active role in early HBe stars. Since early B-type stars do not have large-scale strong magnetic fields, they accrete through the BL mechanism (Lynden-Bell & Pringle 1974). This change in accretion mode for early B-type stars significantly changes the evolution of the circumstellar disk. To decode this, we checked for a correlation between NIR excess and H$\alpha$ EW by segregating them based on the spectral types and found that two distinct populations of early HBe stars exist in the NIR excess and H$\alpha$ EW space. The H$\alpha$ EW for our sample of HBe stars is taken from Vioque et al. (2018). We used the Lada[1] indices to quantify the observed excess in each wavelength regime (Lada 1987). The $IR$ magnitudes were corrected for extinction using respective $A_\lambda$ conversion coefficients from Wang & Chen (2019).

The presence of two sub-populations is visualised in the SED plot (Fig. 1a) with the colour of each line denoting the H$\alpha$ EW of the star. For visual purposes, we normalised the flux values of all the stars at the $J$ band. As seen, for stars with high H$\alpha$ EW (>50 Å), the SED shows excesses at shorter wavelengths ($J$ or $H$ bands). And for stars with low H$\alpha$ EW, the excesses start

---

[1] The equation defining the Lada index is as follows:

$$n_{\lambda_1 - \lambda_2} = \frac{\log(\frac{\lambda_2 F_{\lambda_2}}{\lambda_1 F_{\lambda_1}})}{\log(\frac{\lambda_2}{\lambda_1})}, \tag{1}$$

where $\lambda_1$ and $\lambda_2$ represent the wavelength of two bands for which the spectral index was calculated. Furthermore, $F_{\lambda_1}$ and $F_{\lambda_2}$ represent the extinction-corrected absolute flux measured at $\lambda_1$ and $\lambda_2$, respectively.
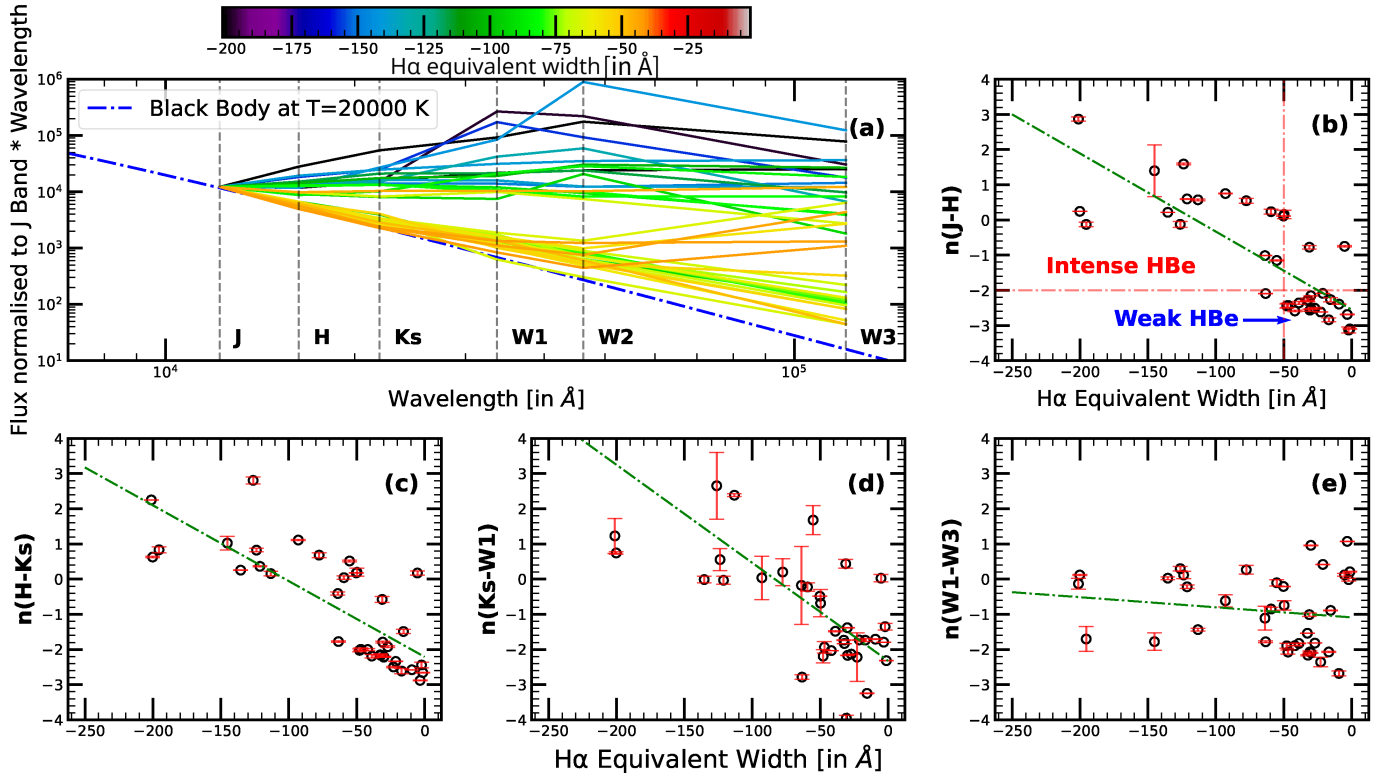
**Fig. 1.** Panel a visualises the NIR excess present in the SED of early HBe stars studied in this work. The colour of each SED represents the Hα emission strength. The dash-dotted line represents the blackbody SED for $T = 20\,000$ K. The flux values were normalised to the *J* band for visual purposes. The mean wavelength of each IR filter is marked using dashed lines. Panels b–e represent the distribution of Lada indices between *IR* magnitudes with respect to the Hα EW. The green dash-dotted lines in panels b–e show a linear fit to the scatter points shown in each plot. The red dash-dotted lines in panel b represent the cutoffs (|Hα EW| = 50 Å and $n$(J–H) = −2) used to separate the intense and weak HBe stars.

at longer wavelengths ($K_S$ or more). Even though some outliers show relatively high NIR excess for low Hα emission strength, the overall trend of stars with high Hα EW having high NIR excess is visible. The presence of two distinct populations is also seen in Figs. 1b,c, which shows the correlation between NIR indices and the Hα EW. It is clear from Figs. 1a–c that two different populations of early HBe stars exist: one with high NIR excess and high Hα EW and the other with low NIR excess and low Hα EW in the sample of early HBe (B0–B5) stars. Since NIR continuum excess is primarily from the inner hot disk, intense NIR emission and its correlation with Hα emission suggests the presence of an inner hot disk. It is still possible that HBes may have high MIR/FIR excess caused by the presence of a dusty outer disk. It should be noted that the MIR excess, evaluated using the $n(K_S - W1)$ and n(W1−W3) indices (Figs. 1d,e), does not distinguish the two populations that are seen in NIR–Hα EW space. It is pertinent to note that the two populations discussed here only differ in the NIR wavelength region and show similar indices in the MIR region, which suggests a similarity in the outer disk of these stars.

For further analysis, we separated the sample of 37 HBe stars into 'intense' and 'weak' HBe stars based on the cutoffs shown in Fig. 1b. The extinction-corrected NIR indices lie close to the photospheric colours for stars with |Hα EW| < 50 Å. We separated the two populations based on median values of the Hα EW and $n$(J−H) Lada index distributions. The cutoffs used to distinguish intense and weak HBes are |Hα EW| = 50 Å and $n$(J−H) = −2. Hence, 15 HBe stars satisfying |Hα EW| > 50 Å and $n$(J−H) > −2 are classified as 'intense HBe' stars and 18 HBe stars with |Hα EW| < 50 Å and $n$(J−H) < −2 are classified as 'weak HBe'

stars. The remaining four stars did not fit under these definitions and hence were removed from further analysis. The basic stellar parameters of 15 intense and 18 weak HBe stars are provided in Table B.1.

It should be noted that non-simultaneity of observation exists between Hα EW, 2MASS, and WISE observations. However, this would not affect our analysis as HBe stars are not highly variable compared to HAe stars (refer to Fig. 8 of Vioque et al. 2018). Moreover, the role of $A_V$ is critical in estimating the NIR excess of the Herbig stars. However, as discussed in Sect. 4.1, the uncertainty in the $A_V$ value does not affect the presence of two sub-populations in NIR excess versus Hα space.

### 3.2. Difference in the spectral features of HBe stars belonging to two sub-populations

In addition to the differences in the NIR excess and Hα EW of the two sub-populations, there exist clear differences in various emission lines that are often found in HAeBe stars. Based on the presence of higher-order HI emission lines in Herbig stars, Shridharan et al. (2023) point out that some young stars lose the dynamic inner circumstellar medium very early in their PMS phase. The difference in the circumstellar medium manifests in the presence or absence, as well as the intensity of spectral lines. Hence, we evaluated the distinction in the spectral lines and features using the VLT/X-shooter spectra. Only 13 out of 37 HBe stars in our list have X-shooter spectra. To maintain the homogeneity in the analysis, we use only the available X-shooter spectrum and do not consider spectra from other instruments. We plan to perform a spectroscopic survey of all 37 HBe stars in
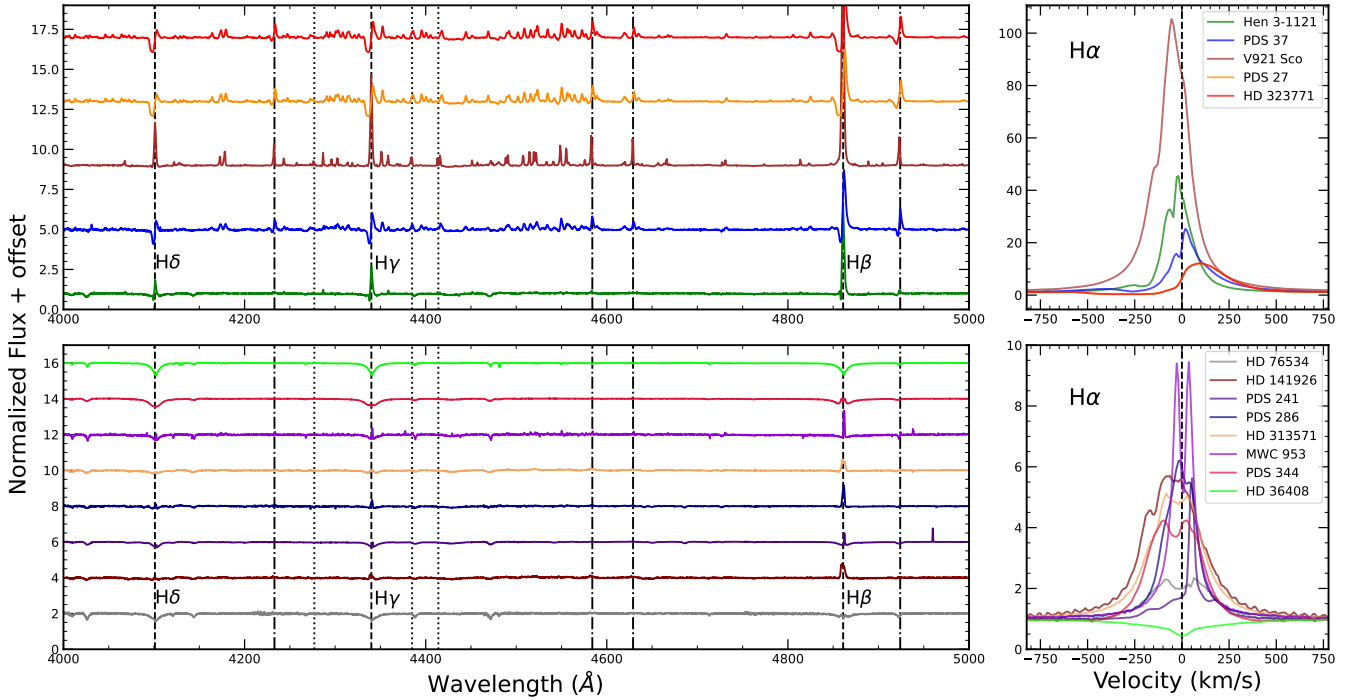
**Fig. 2.** X-shooter spectra showing the differences in Balmer profiles belonging to intense (top panel) and weak (bottom panel) HBe stars. The top left panel shows the higher order Balmer lines, selected FeII (dash-dotted), and [FeII] (dotted) lines present in the spectra of intense HBe stars. The top right panel shows the Hα profiles of intense HBe stars, where the blueshifted absorptions are clearly seen. The bottom panels show the spectra of weak HBes, where the emission lines are feeble compared to intense HBes. The spectra displayed in this work were not corrected for Doppler shift due to the stellar radial velocity.

the future, which is beyond the scope of this work. This section details differences in various spectral features observed in the X-shooter spectrum belonging to five intense and eight weak HBe stars.

### 3.2.1. HI emission lines

Figure 2 shows the differences in Balmer emission lines of intense and weak HBe emitters. Over the years, it has been clear that the Hα profile, especially in the case of PMS stars, is a combination of emission through different mechanisms such as accretion, the disk, and/or winds. Furthermore, it is susceptible to optical depth effects (Kurosawa et al. 2006). We see that the Hα profiles of intense emitters are not symmetrical and show weak blueshifted absorption in all cases (top right panel of Fig. 2). This is different from the profiles of weak emitters, in which most of them show symmetrical double peaks and only one (HD 141926) shows blueshifted absorption. These profile variations also indicate differences in the inner circumstellar environment of HBe stars, similar to what we assessed from the SED analysis. The blueshifted absorptions are seen at velocities of ∼150–300 km s$^{-1}$, similar to the wind velocities reported in Cauley & Johns-Krull (2015). These differences are not only seen in Hα but also in Hβ and Hγ lines (Fig. 3). The detection of blueshifted absorption features and the non-detection of redshifted absorption features in HBe stars suggests the possibility of BL being the favourable accretion mechanism (Cauley & Johns-Krull 2015).

In addition, we explored the advantage of X-shooter spectra to study the profiles of Paschen and Brackett lines observed during the same epoch, which are shown in Figs. 4 and 5, respectively. We see that the blueshifted features are not prominent in

Paβ, Paγ, and Brγ lines (Fig. 3), suggesting that these features can be wavelength dependent and/or due to the contribution from different emission regions. However, the blueward asymmetry is still present in the lower-order lines of the Paschen and Brackett series. It should be noted that in the case of higher-order lines of the Paschen series, the asymmetry in the profiles can be seen to an extent. However, the asymmetry completely disappears for higher-order lines of the Brackett series. This again points to the wavelength-dependent opacity of the medium, causing the blueshifted absorption. Interestingly, there is no distinction between intense and weak emitters when it comes to the presence of higher-order lines of the Brackett series (Fig. 5).

### 3.2.2. FeII emission lines

HAeBe stars show emission lines belonging to metallic species such as FeII, CaII triplet, OI, and [OI] lines in their spectra (Hamann & Persson 1992a). We also observe differences in intense and weak emitters based on the presence of these metallic lines. FeII lines (particularly those present in the UVB arm of X-shooter spectra) are seen in emission in intense HBe stars, whereas they are completely absent in weak emitters (Fig. 2). Since FeII lines (especially 4924 Å) are seen in P-Cygni morphology in three out of five intense emitters, they may arise from a region of outflow. Furthermore, many weak emission lines in the wavelength range 4350–4650 Å of intense HBe stars are completely absent in weak HBe stars.

### 3.2.3. CaII emission lines

CaII triplet lines (8498 Å, 8542 Å, and 8662 Å) require lower energy for ionisation and can form in cooler regions of the
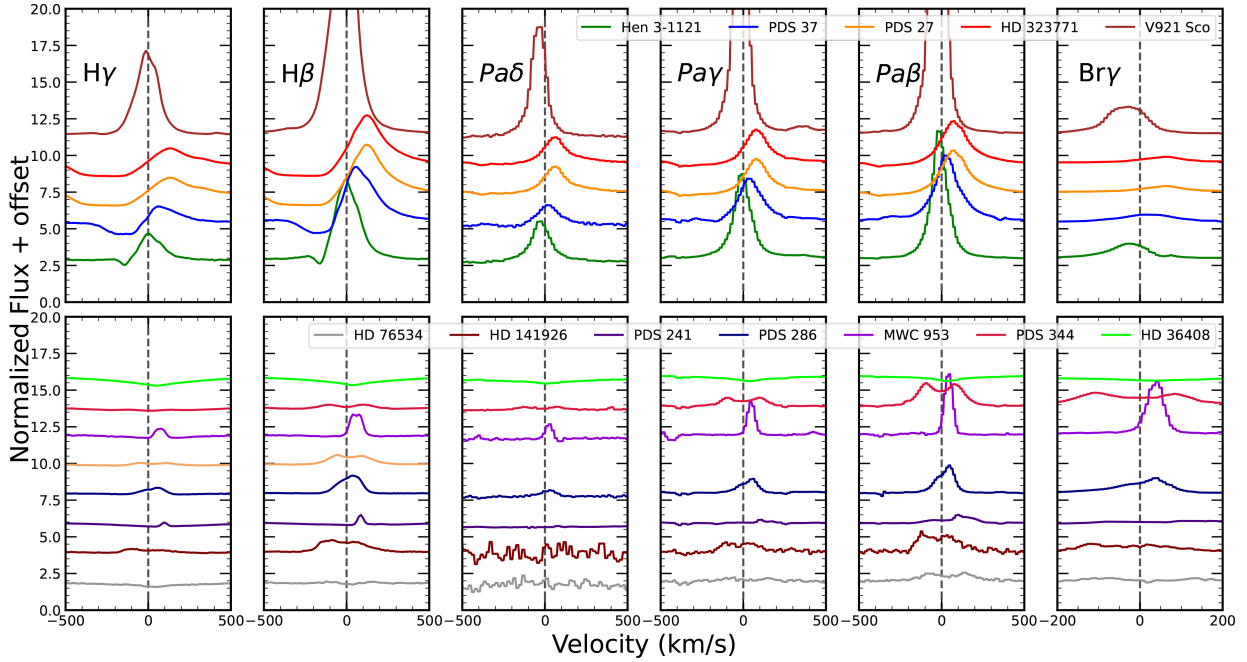
**Fig. 3.** X-shooter spectra showing the profiles of lower-order HI lines belonging to intense (top panel) and weak (bottom panel) HBe stars. The blueshifted absorption feature is seen in the Balmer lines. However, the contribution of blueshifted absorption decreases as we move to Paschen and Brackett lines, denoting the wavelength-dependent opacity of the absorbing medium.
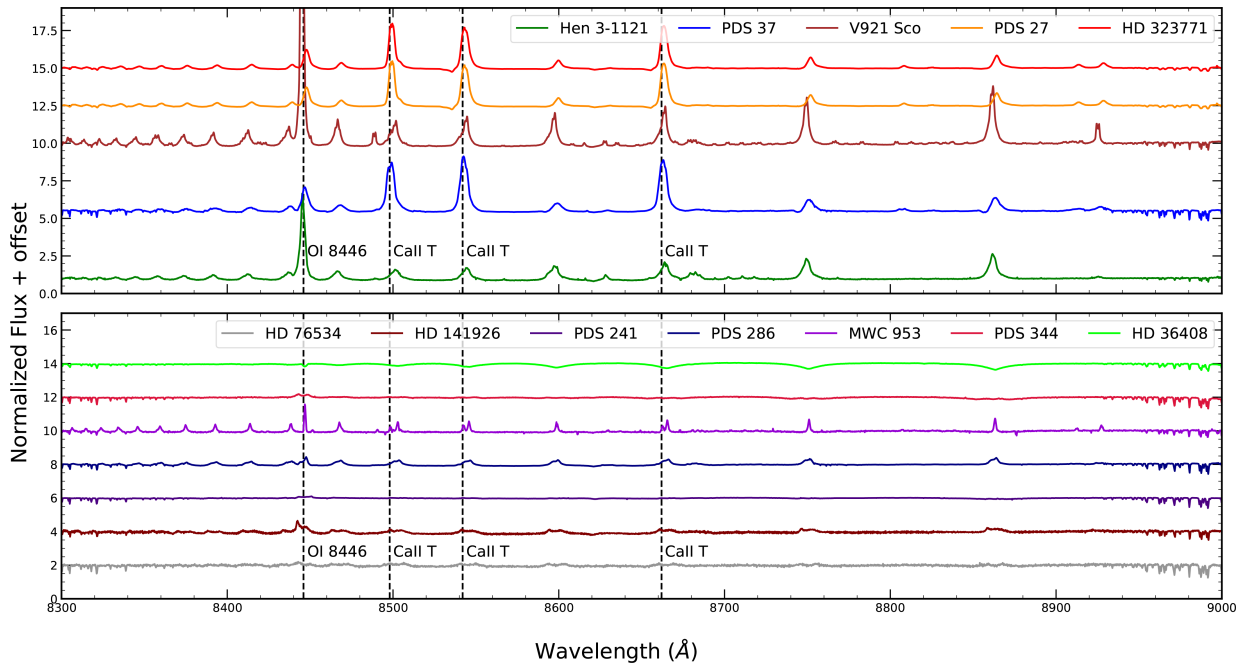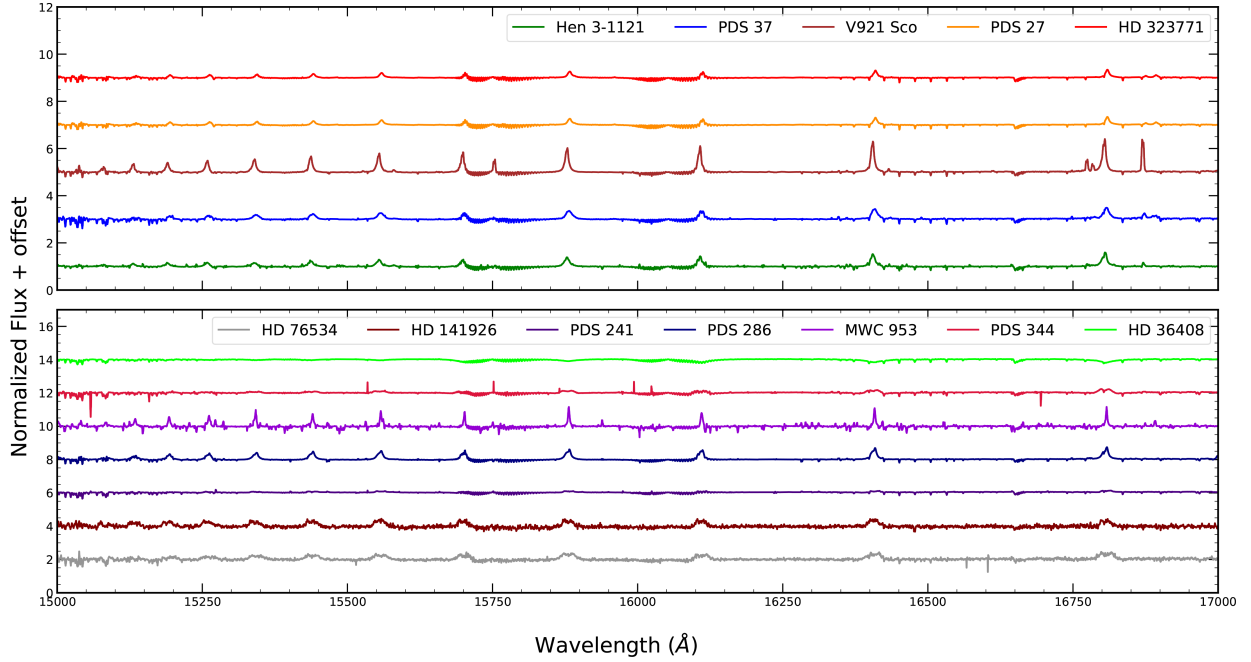


**Fig. 4.** X-shooter spectra showing the differences in Paschen and CaII triplet profiles belonging to intense (top panel) and weak (bottom panel) HBe stars. The OI 8446 Å and CaII triplet lines are marked with dashed lines. The difference in intensity of the emission lines can be seen between the top and bottom panels.

circumstellar disk. CaII triplet lines are seen in three (out of five) intense emitters and in one (MWC 953) of the weak emitters (Fig. 4). Hamann & Persson (1992a) studied the CaII triplet emission in HAeBe stars and noted that 71% of the HBe stars show CaII triplet in emission. They propose that the CaII triplet emission should come from denser regions of the hot star. The low-ionisation energy (energy of the upper level in the transition [$E_{upper}$] ∼ 3.1 eV) of the triplet means they arise from cooler regions away from the star and may not be associated

with the inner hot gaseous disk. Further, the observed ratios of CaII triplet emission is 1:1:1 instead of ∼1:10:6, as expected by the ratio of oscillator strengths (log(gf))[2]. Hence they arise from an optically thick region. It is also interesting to note that three stars showing a CaII triplet also show CaII doublet emission (8912 Å and 8927 Å). The CaII doublet ratio is also close

---

[2] https://physics.nist.gov/PhysRefData/ASD/lines_form.html

**Fig. 5.** X-shooter spectra showing the differences in higher-order lines of Brackett series belonging to intense (top panel) and weak (bottom panel) HBe stars. It is interesting to see that the higher-order Brackett series lines are of comparable intensities between intense and weak HBes in contrast to all of the other emission lines.

to unity with 8927 Å being slightly more intense than 8912 Å. As discussed in Hamann & Persson (1992b), the CaII may be arising due to greater saturation of triplet lines caused by the optical thickness of the CaII emitting medium. The difference in energy levels of CaII triplet ($E_{upper} \sim 3.1$ eV) and doublet ($E_{upper} \sim 8.4$ eV) lines points to different regions of line formation. Interestingly, a weak HBe star, MWC 953, shows both CaII triplet and CaII doublet lines in emission; although, it is weak compared to intense emitters).

### 3.2.4. OI emission lines

Mathew et al. (2018) show that the most likely excitation mechanism for the formation of OI lines is Ly$\beta$ fluorescence. They observed that the emission strengths of 8446 Å and 11287 Å are more intense than the adjacent OI lines at 7774 Å and 13165 Å. We observed OI lines in emission in all five intense HBe stars and one (MWC 953) of the weak emitters (Fig. 6). It should be noted that CaII triplet emission and OI lines seen in MWC 953 are weaker and narrower compared to the lines observed in intense emitters. For intense HBe stars, V921 Sco and Hen 3-1121, the ratio of the observed pair of lines (8446/7774 and 13165/11287) follows the ratio observed in Mathew et al. (2018). The observed [log(F(8446)/F(7774)), log(F(11287)/F(13165)] ratios are [0.79, 0.68] and [0.59, 0.74] for V921 Sco and Hen 3-1121, respectively[3]. We also note that the intensity of OI directly correlates with the spectral type. The intensity is maximum for V921 Sco (B0-B1), which falls off for Hen 3-1121 (B1-B2) and eventually becomes negligible for PDS 37 (B2-B3). The OI lines (especially the IR lines) are non-existent for PDS 27 and HD 323771 (B4-B5). Considering [OI] lines, which are used as wind indicators in HAeBe stars (Corcoran & Ray 1998), we see that V921 Sco, PDS 37, and HD 323771 show both 6300 Å and

6363 Å lines. The rest of the stars studied do not show [OI] in emission.

### 3.2.5. HeI 10830 Å emission feature

More importantly, the meta-stable HeI 10830 emission line is used as a probe to study the dynamics of mass flows around HAe/Be stars (Cauley & Johns-Krull 2014). The blueshifted features observed in HI lines are also seen in the HeI 10830 Å line of intense HBe stars (Fig. 6). The blueshifted ($\sim$150–300 km s$^{-1}$) HeI 10830 Å line mimicking the blueshifted feature in Balmer profiles shows that the absorption mechanisms in both cases can be physically related. Hence, the blueshifted absorption feature in Balmer lines may come from stellar wind in the inner circumstellar region or an expanding envelope along the line of sight to the star, which is missing in weak HBes.

## 4. Discussion

### 4.1. Role of $A_V$

Since B-type stars evolve rapidly and reach the main sequence faster than A-type stars, HBe stars are more likely to be associated with the pre-natal cloud. Hence, the line-of-sight extinction can be higher towards the early-type stars. The estimation of $A_V$ towards the early B type depends on identifying accurate spectral type using high-resolution spectra. Hence, the $A_V$ estimation always carries an inherent uncertainty. To ensure that the NIR excess estimates are not influenced due to the underestimation or overestimation of the $A_V$ value, we varied the $A_V$ by 25% and 50% to see the change in the indices. Figure 7 shows the change in indices if the $A_V$ was varied. We can see that even if the $A_V$ was varied by 50%, the Lada indices do not vary significantly. The pattern of two populations in $n$(J−H) is still valid even if the $A_V$ is under or overestimated by 50%. Hence, the $A_V$ value used in this study does not affect the identification of two subpopulations in early HBe stars. The NIR excess seen in intense

---

[3] We did not measure ratios for other intense HBe stars since OI lines show a p-cygni profile, which can affect the calculation.
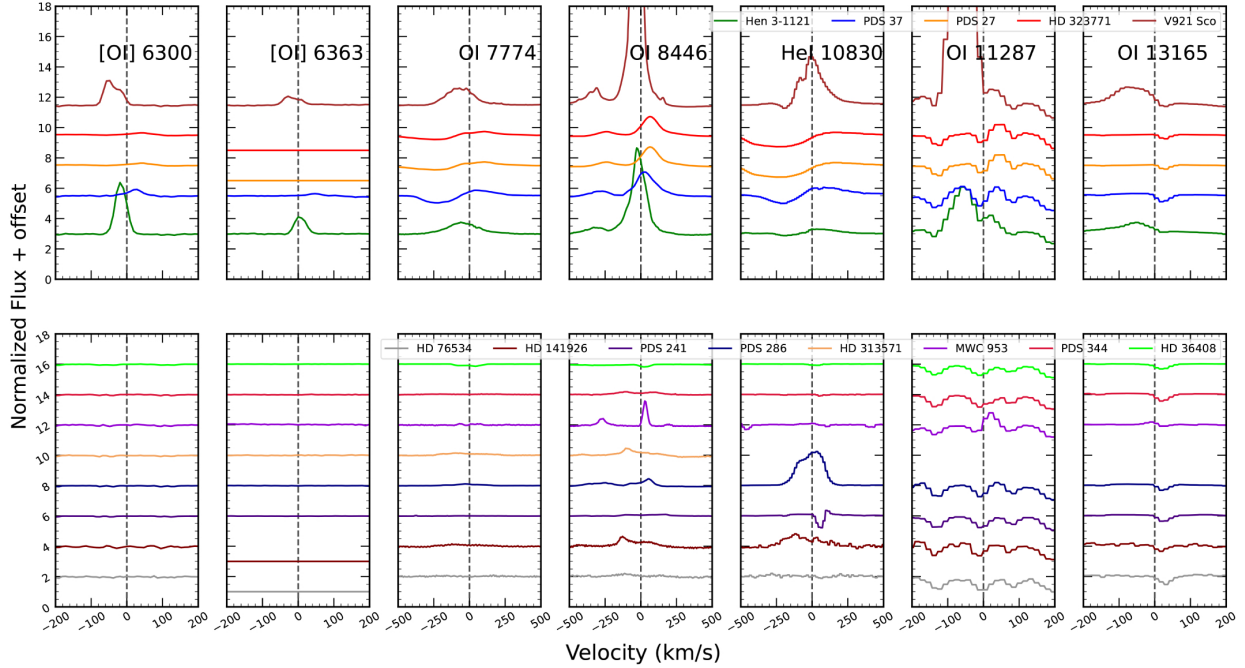
**Fig. 6.** X-shooter spectra showing the differences in metallic lines belonging to intense (top panels) and weak (bottom panels) HBe stars. The stark contrast between intense and weak emitters is clear based on the presence of OI 7774 Å, 8446 Å, 11287 Å, and 13165 Å lines. The HeI 10830 Å lines of intense HBe stars show blueshifted absorption, similar to their Balmer profiles.
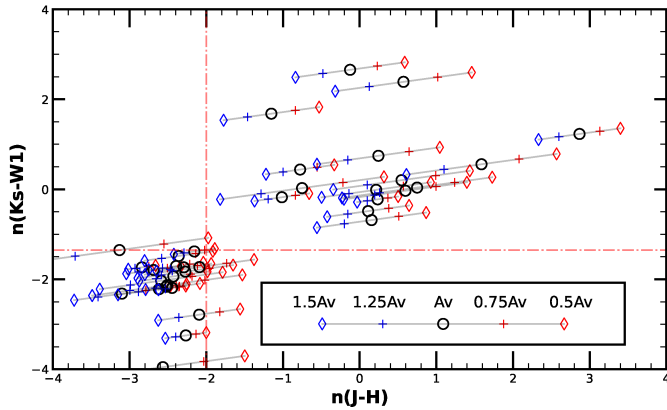


**Fig. 7.** Scatter plot of Lada indices $n$(J−H) and n(K$_S$ −W1) for the HBe stars studied in this work. The A$_V$ was varied by 25% and 50%, and the resultant index values are marked with plus and diamond symbols, respectively. The symbols are marked in blue if the A$_V$ was increased and in red if the A$_V$ was decreased. The inset subplot explains the symbols and colours used in the plot with the respective A$_V$ value above each symbol.

HBe stars is genuine and is not affected by the uncertainty in the A$_V$ parameter.

### 4.2. Bimodality in accretion rates

There are important studies (e.g. Mendigutía et al. 2011a; Arun et al. 2019 and Wichittanakom et al. 2020) that have estimated the accretion rates of HBe stars homogeneously using H$\alpha$ EW values. Using the correlation between accretion rates and stellar mass, Wichittanakom et al. (2020) show that the accretion mode changes at around 4 $M_\odot$. It also can be seen from their analysis (Fig. 7, right, of Wichittanakom et al. 2020) that there exists a large scatter in the mass accretion rates of HBe stars. Although there exists no clear distinction, we can see that the range of

mass accretion rates can vary from $10^{-7}$ to $10^{-3}$ $M_\odot$ yr$^{-1}$. However, as mentioned, the H$\alpha$ emission line has many contributions and suffers from opacity issues. As seen from the H$\alpha$ profiles of intense HBe stars, there is a blueshifted absorption component, which reduces the total H$\alpha$ strength and underestimates the mass accretion rate. It is possible to overcome the opacity issue using the Br$\gamma$ line, as proposed by Grant et al. (2022). As pointed out by them, there is a change in slope of log ($\dot{M}_{acc}$) versus log($M_\star$) plot for high-mass objects when compared with low-mass HAes. Though there is no direct sample overlap between our work and Grant et al. (2022), we point to Fig. 11 of Grant et al. (2022). The figure mimics our finding that two different populations exist in mass accretion rate values for stars belonging to the B0–B5 spectral range. The $\dot{M}_{acc}$ values in Grant et al. (2022) for early HBe stars ranges from $10^{-7}$ to $10^{-3}$ $M_\odot$ yr$^{-1}$. One set of early HBe stars have $\dot{M}_{acc}$ in the range of $10^{-4.5}$ to $10^{-3}$ $M_\odot$ yr$^{-1}$ and another set of stars have values in the range $10^{-6}$ to $10^{-7}$ $M_\odot$ yr$^{-1}$. Under the assumption that Br$\gamma$ emission directly correlates with the mass accretion rate, the two to three orders of magnitude difference in the mass accretion rates between the two populations is evidence of intense HBe stars undergoing accretion through BL and that the active accretion phase has ended in weak HBe stars.

### 4.3. Spectral features observed in other spectral ranges

The interesting spectral features seen in intense HBe stars, such as FeII and [FeII] lines in the $UVB$ band of X-shooter spectra, are not limited to this spectral type. We checked all the X-shooter spectra of Herbig stars to see the incidence of intense FeII and [FeII] emission lines. We note that stars belonging to B5-B9 (HD 259431, PDS 133, and HD 85567) and A0-A5 (V380 Ori and Z CMa) also show spectral features similar to intense HBe stars. Interestingly, some of these stars have been studied in detail using various techniques. The stars V380 Ori and Z CMa are known to be associated with Herbig-Haro outflows and bipolar jets (Whelan et al. 2010; Reipurth et al. 2013).

HD 85567 and HD 259431 stars are shown to have an inner compact gaseous disk with a size <1 au (Kraus et al. 2008; Bagnoli et al. 2010; Wheelwright et al. 2013). Even though they belong to later spectral types, the commonality between the spectral features could mean that the properties of the emission medium can be identical. This can be considered as indirect evidence for the presence of inner gaseous disks and intense outflows in the sample of intense HBe stars.

### 4.4. Comparison with other types of Be stars

A natural question as to the classification of weak HBe stars is whether they truly belong to the Herbig category. Given the mass range of B0–B5 stars (5–18 $M_\odot$), they typically stay in the PMS phase for less than 2 Myr (MIST; Dotter 2016; Choi et al. 2016). Hence, finding them in the PMS phase is difficult due to the rapid evolutionary timescales. Thus, the validity of these massive stars being in the Herbig phase is always under scrutiny.

Since the photometric and spectroscopic signatures of weak HBes and classical Be (CBe) stars are very similar, CBe stars may be masquerading as the weak HBes in our sample. Similarly, over the years, stars such as MWC 137, which are classified as young HBe stars, turned out to be evolved supergiant stars by recent studies (Kraus et al. 2021). In the context of intense HBe stars, it is essential to mention the stars classified in the literature as 'B-type stars showing B[e] phenomenon'. B[e] phenomenon was described by Lamers et al. (1998) as B-type stars showing high NIR excess and intense Hα emission along with allowed and forbidden (especially [OI], [FeII], and [NII]) emission lines in their spectra. The B[e] phenomenon does not occur at a particular evolutionary stage. Instead, it has been observed in PMS stars, supergiants, symbiotic binaries, and planetary nebulae (PNe). Furthermore, B[e] stars are highly reddened, and their spectra do not show any photospheric lines. It has been shown by De Winter et al. (1998) that stars showing B[e] are not part of young clusters or nebulosity. The similarity in spectral and NIR characteristics of our intense HBes and B[e] stars can affect the classification. Hence, the validity of the young nature of our HBe sample needs to be rechecked. In this section, we assess the information available in the literature to confirm the HBe nature of our sample of stars.

*Intense HBe stars.* Hen 3-1121 has been confirmed to be a young HAeBe star by Carmona et al. (2010) through high-resolution spectroscopy. PDS 37 and 27 are reported to be massive YSO stars undergoing intense accretion ($10^{-3}$ to $10^{-4.5}$ $M_\odot$ yr$^{-1}$) and are on track to become O-type stars. They are observed to have a flattened inner disk structure (Ababakr et al. 2015). V921 Sco was first classified as a Bep supergiant star by Hutsemekers & van Drom (1990). However, due to the non-detection of the CO bandhead and the observed emission region of Brγ, it is classified as a PMS star by Kraus et al. (2012a). There is no relevant literature about HD 323771 star, except that it is of B5V spectral type (Vieira et al. 2003).

*Weak HBe stars.* There has been considerable ambiguity regarding the evolutionary phase of HD 76534 in the literature. It belongs to the Vela R2 association (Herbst 1975), which is a young star formation region, and the star has a nebular region associated with it. Recently, by modelling the circumstellar disk, Patel et al. (2017) suggested the presence of a passive, optically thick disk. From interferometric studies, it has been suggested that HD 141926 possibly accretes through the BL mechanism (Marcos-Arenal et al. 2021). PDS 241 was suggested to be a CBe star due to its low MIR flux (Verhoeff et al. 2012), but

it has been studied as a HAeBe star in the recent works of Guzmán-Díaz et al. (2021) and Grant et al. (2022). HD 313571 and MWC 953 are confirmed as HAeBe stars by high-resolution optical spectroscopy (Carmona et al. 2010). They are also known to be associated with nebulosity in *Spitzer* images. There are no relevant literature about the nature of PDS 286 and HD 36408.

It should be noted that there is no distinction between the intense and weak HBe stars based on age, mass, and luminosity values (based on the values listed in Guzmán-Díaz et al. 2021). Hence, it could be said that the intense and weak HBe stars belong to similar evolutionary phases. However, we are aware of the caveat here that the characteristics of intense HBe stars, such as intense HI emission, [FeII] emission, and blueshifted absorption features in HI lines, are observed in supergiant B[e] (sgB[e]) stars as well (Lamers et al. 1998). A fail-safe method to distinguish HBe and sgB[e] stars is through the detection of the $^{13}$CO bandhead emission and ratio of $^{12}$CO/$^{13}$CO features (Kraus 2009). Hence, high-resolution *K*-band spectroscopy is required to confirm the validity of the young nature of the intense HBe stars. In addition, V921 Sco is identified to have a very close (~0.025″) late B-type companion star through interferometry (Kraus et al. 2012b). They suggest that the B[e] phenomenon observed in V921 Sco is a consequence of binary interactions, where the forbidden-line emitting material gets ejected during the episodic interaction phases. Thus, it could be possible to explain the features of intense HBe stars through an interaction with their undetected close binary companions. Since previous studies indicate that most of the intense and weak HBe stars are found to be young and associated with the nebulosity, we have treated them as young PMS stars in this work.

## 5. Summary and conclusions

In this work, we made use of the archival photometric and spectroscopic data available for early HBe stars to study the two sub-populations within the sample of early HBe stars. We analyse the correlation between NIR excess and Hα emission strength, supported by the distinction in the spectral features, to show that the inner circumstellar medium belonging to intense and weak HBe stars is different. Though there have been indications for two sub-populations of early HBe stars, this is the first work to point out the clear differences between them using IR photometry and various spectroscopic features using VLT/X-shooter spectra. The major results are summarised below.

- The NIR excess, as quantified by the $n$(J−H) Lada index, shows that one population of HBe stars has weak NIR excess, whereas the other population of HBe stars has very high NIR excess. Since the NIR excess corresponds to the inner circumstellar medium of the Herbig star, the dichotomy between the populations also corresponds to the difference in the evolution of the inner circumstellar medium.
- Furthermore, the stars with high NIR excess also seem to show higher Hα EW and vice versa. The emission strength of Hα has always been directly used to estimate the mass accretion rate in PMS stars. The high Hα EW values thus also correspond to a higher rate of accretion in these stars.
- Since the early HBe stars are known to accrete through the BL mechanism, we propose that the difference in Hα and NIR excess indirectly points to two types of early HBe stars – those HBe stars with an inner disk and accreting through the BL mechanism, and a second population with an evolved circumstellar medium where the BL accretion has stopped.
- This is also supported by the differences in the spectral features seen in X-shooter spectra for a sub-sample of HBe

stars. Most importantly, the Hα profiles of all intense HBe stars show blueshifted absorption features. However, in the weak HBe stars, the Hα profiles are symmetrical.

– The blueshifted absorption in intense HBe stars is also seen in other HI lines such as Hβ, Paβ, and Brγ. It should be noted that the blueshifted absorption is not relatively well pronounced in Brackett and Paschen lines, but the blueward asymmetry of the profiles is clear.

– The metallic lines, OI, [OI], and CaII triplet often seen in HAeBe stars also show the distinction between intense and weak HBes. We note that OI 7774 Å, 8446 Å and [OI] 6300 Å, 6363 Å lines are only present in intense HBe and completely absent in weak HBe. Since [OI] lines form due to outflows from the star, it can be concluded that there are no stellar winds or outflows from weak HBe stars.

– We note that HeI 10830 Å, a meta-stable transition line, has been studied extensively by Cauley & Johns-Krull (2014, 2015) to estimate accretion and mass flow around Herbig stars. The non-detection of blueshifted HeI 10830 Å in weak HBe shows no mass flow from the star. It acts as an indirect indicator of dampened activity in the circumstellar medium of weak HBe stars. The blueshifted velocities of the HeI 10830 Å absorption feature also correspond with the blueshifted velocities seen in Hα and Hβ profiles in intense HBe stars.

– Many lines belonging to different multiplets of FeII and [FeII] transitions are seen in the wavelength range 4200–4450 Å in intense HBe stars and are absent in the weak HBe stars. Another interesting spectral feature we noted is the presence of CaII doublet lines at 8912 Å and 8927 Å in three intense HBe stars.

– Most of the stars used in this study are classified as HBe stars from extensive, independent studies. Hence, the possibility of B[e] stars and CBe stars being classified as intense HBe and weak HBe, respectively, can be neglected.

– We have identified 44 intense HBe candidates from the latest *Gaia* DR3 database. A detailed spectroscopic analysis is necessary to confirm the intense HBe nature of these 44 candidates (Appendix A).

This work points to the several differences that exists between the two sub-populations of early HBe stars and proposes that the distinction is due to difference in their inner circumstellar caused by evolution of disk undergoing accretion through BL. However, we are aware that these differences can be explained by other causes such as binary interactions. To understand the population of intense HBe stars better, we plan to perform high angular resolution interferometry and high-resolution *K*-band spectroscopy in the near future.

# References

Ababakr, K., Fairlamb, J., Oudmaijer, R., & van den Ancker, M. 2015, MNRAS, 452, 2566

Acke, B., Verhoelst, T., Van den Ancker, M., et al. 2008, A&A, 485, 209

Arun, R., Mathew, B., Manoj, P., et al. 2019, VizieR Online Data Catalog: J/AJ/157/159

Bagnoli, T., Van Lieshout, R., Waters, L., et al. 2010, ApJ, 724, L5

Bailer-Jones, C., Rybizki, J., Fouesneau, M., Demleitner, M., & Andrae, R. 2021, AJ, 161, 147

Banzatti, A., Garufi, A., Kama, M., et al. 2018, A&A, 609, L2

Banzatti, A., Abernathy, K. M., Brittain, S., et al. 2022, AJ, 163, 174

Barentsen, G., Farnhill, H. J., Drew, J., et al. 2014, MNRAS, 444, 3230

Brittain, S. D., Kamp, I., Meeus, G., Oudmaijer, R. D., & Waters, L. 2023, Space Sci. Rev., 219, 7

Carmona, A., Van Den Ancker, M., Audard, M., et al. 2010, A&A, 517, A67

Cauley, P. W., & Johns-Krull, C. M. 2014, ApJ, 797, 112

Cauley, P. W., & Johns-Krull, C. M. 2015, ApJ, 810, 5

Choi, J., Dotter, A., Conroy, C., et al. 2016, ApJ, 823, 102

Cohen, M. 1980, MNRAS, 191, 499

Corcoran, M., & Ray, T. 1998, A&A, 331, 147

Cutri, R. M., Wright, E. L., Conrow, T., et al. 2021, VizieR Online Data Catalog: II/328

De Winter, D., Van Den Ancker, M., & Pérez, M. 1998, in B[e] Stars: Proceedings of the Paris Workshop held from 9–12 June, 1997, 1st edn. (Springer), 21

Dotter, A. 2016, ApJS, 222, 8

Drew, J., Busfield, G., Hoare, M., et al. 1997, MNRAS, 286, 538

Fairlamb, J. R., Oudmaijer, R. D., Mendigutía, I., Ilee, J. D., & van den Ancker, M. E. 2015, MNRAS, 453, 976

Fouesneau, M., Frémat, Y., Andrae, R., et al. 2023, A&A, 674, A28

Gaia Collaboration (Vallenari, A., et al.) 2023, A&A, 674, A1

Grant, S. L., Espaillat, C. C., Brittain, S., Scott-Joseph, C., & Calvet, N. 2022, ApJ, 926, 229

Gregory, S., Donati, J.-F., Morin, J., et al. 2012, ApJ, 755, 97

Guzmán-Díaz, J., Mendigutía, I., Montesinos, B., et al. 2021, A&A, 650, A182

Hamann, F., & Persson, S. 1992a, ApJS, 82, 285

Hamann, F., & Persson, S. 1992b, ApJ, 394, 628

Herbig, G. H. 1960, ApJS, 4, 337

Herbst, W. 1975, AJ, 80, 683

Hillenbrand, L. A., Strom, S. E., Vrba, F. J., & Keene, J. 1992, ApJ, 397, 613

Hutsemekers, D., & van Drom, E. 1990, A&A, 238, 134

Kluska, J., Berger, J.-P., Malbet, F., et al. 2020, A&A, 636, A116

Kraus, M. 2009, A&A, 494, 253

Kraus, S., Preibisch, T., & Ohnaka, K. 2008, ApJ, 676, 490

Kraus, S., Calvet, N., Hartmann, L., et al. 2012a, ApJ, 752, 11

Kraus, S., Calvet, N., Hartmann, L., et al. 2012b, ApJ, 746, L2

Kraus, M., Liimets, T., Moiseev, A., et al. 2021, AJ, 162, 150

Kurosawa, R., Harries, T. J., & Symington, N. H. 2006, MNRAS, 370, 580

Lada, C. J. 1987, in Symposium-International Astronomical Union (Cambridge University Press), 115, 1

Lamers, H. J., Zickgraf, F.-J., de Winter, D., Houziaux, L., & Zorec, J. 1998, A&A, 340, 117

Lynden-Bell, D., & Pringle, J. E. 1974, MNRAS, 168, 603

Malfait, K., Bogaert, E., & Waelkens, C. 1998, A&A, 331, 211

Manoj, P., Bhatt, H., Maheswar, G., & Muneer, S. 2006, ApJ, 653, 657

Marcos-Arenal, P., Mendigutía, I., Koumpia, E., et al. 2021, A&A, 652, A68

Mathew, B., Manoj, P., Narang, M., et al. 2018, ApJ, 857, 30

Mendigutía, I. 2020, Galaxies, 8, 39

Mendigutía, I., Calvet, N., Montesinos, B., et al. 2011a, A&A, 535, A99

Mendigutía, I., Eiroa, C., Montesinos, B., et al. 2011b, A&A, 529, A34

Patel, P., Sigut, T., & Landstreet, J. 2017, ApJ, 836, 214

Prusti, T., De Bruijne, J., Brown, A. G., et al. 2016, A&A, 595, A1

Reipurth, B., Bally, J., Aspin, C., et al. 2013, AJ, 146, 118

Shridharan, B., Mathew, B., Bhattacharyya, S., et al. 2022, A&A, 668, A156

Shridharan, B., Mathew, B., Arun, R., & Cysil, T. 2023, JApA, 44, 62

Skrutskie, M. F., Cutri, R. M., Stiening, R., et al. 2006, AJ, 131, 1163

Strom, S. 1972, PASP, 84, 745

Verhoeff, A., Waters, L., Van den Ancker, M., et al. 2012, A&A, 538, A101

Vieira, S. L. A., Corradi, W. J. B., Alencar, S. H. P., et al. 2003, AJ, 126, 2971

Villebrun, F., Alecian, E., Hussain, G., et al. 2019, A&A, 622, A72

Vioque, M., Oudmaijer, R., Baines, D., Mendigutía, I., & Pérez-Martínez, R. 2018, A&A, 620, A128

Vioque, M., Oudmaijer, R., Schreiner, M., et al. 2020, A&A, 638, A21

Wang, S., & Chen, X. 2019, ApJ, 877, 116

Wheelwright, H., Weigelt, G., o Garatti, A. C., & Lopez, R. G. 2013, A&A, 558, A116

Whelan, E., Dougados, C., Perrin, M., et al. 2010, ApJ, 720, L119

Wichittanakom, C., Oudmaijer, R., Fairlamb, J., et al. 2020, MNRAS, 493, 234

Zickgraf, F.-J. 2003, A&A, 408, 257

# Appendix A: Identification of new intense HBe candidates from *Gaia* DR3

As shown in previous sections, two distinct populations of massive Herbig stars seem to have drastically different inner circumstellar environments. The works of HAeBe stars over the years have been skewed towards late HBe and HAe stars. Only in the recent works (e.g. Guzmán-Díaz et al. 2021; Mendigutía et al. 2011a) has effort been made to include more HBe stars into the analysis. Using the latest *Gaia* DR3 (Gaia Collaboration 2023), it is possible to identify new intense HBe candidates. *Gaia* DR3 provides spectroscopic parameters for 2.3 million hot stars and a catalogue of 57,511 emission-line stars based on the pseudo-equivalent width (pEW) measurements (Fouesneau et al. 2023). The catalogue provides various ELS classes such as 'beStar', 'TTauri', 'HerbigStar', and 'PN' based on their BP/RP spectra. We used the ELS catalogue given by *Gaia* DR3 and 2MASS colours to search for more intense HBe candidates. In order to search for new intense HBe stars from *Gaia* DR3, we queried the ELS catalogue using the *Gaia* ADQL facility. We cross-matched the stars classified as 'HerbigStar' in *Gaia* DR3 with the 2MASS catalogue and got 3825 sources. Shridharan et al. (2022) propose a second-order polynomial to convert pseudo-EW to observed H$\alpha$ EW of emission-line stars. We used the highest piece-wise fit parameter values in Fig. 3 of Shridharan et al. (2022) to estimate the observed H$\alpha$ EW of the stars. Then, 325 stars with the estimated |H$\alpha$ EW| > 50 Å were retained. To find the hot stars from this sample, we selected those stars with *teff_gspphot* > 15 000 K. The estimate *teff_esphs* was not used because it was not available for a significant fraction of our candidate objects. After the *teff_gspphot* cutoff, 65 stars were retained. Further, $n$(J−H) was estimated for these 65 sources using the extinction value provided by *Gaia* DR3. Finally, we identified 44 potential intense HBe candidates from this analysis. Of 44 candidates, 36 are already recorded in the SIMBAD database. A table containing information regarding the possible intense HBe candidates is provided in Table A.1. Even though *Gaia* DR3 has classified these stars as 'HerbigStar', one should be cautious about accepting this classification. Some stars given in Table A.1 may belong to PNe and supergiant phases. Through this section, we intend to demonstrate the use of large-scale surveys such as *Gaia* to identify interesting set of objects such as intense HBe stars. A detailed and careful spectroscopic study is needed to prove the young nature of these stars.

**Table A.1.** Table containing information about the intense HBe candidates identified from *Gaia* DR3.

| Gaia_Source_ID | RA | Dec | Gaia_ClassELS | $A_G$ | Distance (in pc) | $T_{eff}$(K) | pEWHa(nm) | EWHa_conv(Å) | n(J-H) | Simbad_ID |
|---|---|---|---|---|---|---|---|---|---|---|
| 2065600343226602112 | 313.5307746 | 41.5827610 7 | HerbigStar | 4.5 | $771^{+9}_{-9}$ | 19,437 | -3.06 | -76.27 | 1.36 | V* V1219 Cyg |
| 5864938685013848320 | 202.1618059 | -63.82954127 | HerbigStar | 3.2 | $5076^{+162}_{-335}$ | 15,012 | -13.78 | -331.44 | 1.11 | PN Th 2-B |
| 5258349561694308096 | 151.1261185 | -58.66444562 | HerbigStar | 2.9 | $984^{+30}_{-39}$ | 19,161 | -5.34 | -130.47 | 0.98 | HD 87643 |
| 2020112789377651712 | 296.0219088 | 23.4466286 | HerbigStar | 3.6 | $2716^{+100}_{-57}$ | 19,503 | -10.7 | -257.98 | 0.7 | Hen 2-446 |
| 2170966574983202560 | 322.0225077 | 49.68336095 | HerbigStar | 2.5 | $2345^{+176}_{-41}$ | 15,009 | -2.33 | -58.81 | 0.67 | EM* GGR 25 |
| 4661416379669398144 | 77.40419259 | -67.91911637 | HerbigStar | 0.8 | $16807^{+289}_{-273}$ | 17,370 | -6.48 | -157.68 | 0.47 | 2MASS J05093702-6755086 |
| 6053784647417889280 | 185.5965192 | -63.28801792 | HerbigStar | 3.0 | $3381^{+399}_{-948}$ | 15,539 | -5.84 | -142.52 | 0.45 | WRAY 16-110 |
| 4103969761134412544 | 277.4986 | -14.94720448 | HerbigStar | 2.5 | $2819^{+128}_{-67}$ | 20,803 | -12.43 | -299.19 | 0.31 | SS 389 |
| 5868482307854016000 | 200.0148814 | -62.39835807 | HerbigStar | 1.9 | $5836^{+48}_{-47}$ | 15,948 | -2.98 | -74.51 | 0.03 | THA 17-35 |
| 5980805834434317184 | 239.5400967 | -53.85511504 | HerbigStar | 3.6 | $4028^{+544}_{-682}$ | 30,636 | -4.72 | -115.69 | -0.01 | WRAY 15-1390 |
| 5601822631829205376 | 117.1625314 | -26.67784839 | HerbigStar | 2.2 | $7641^{+5}_{-4}$ | 17,363 | -2.33 | -58.97 | -0.07 | SS 162 |
| 4650950785570772864 | 82.87780386 | -71.74670027 | HerbigStar | 1.1 | $12426^{+311}_{-330}$ | 17,340 | -5.59 | -136.55 | -0.07 | SSTISAGEMC J053130.65-714448.2 |
| 5972815515955517696 | 260.2314013 | -38.00011208 | HerbigStar | 4.8 | $2078^{+94}_{-98}$ | 28,514 | -6.64 | -161.56 | -0.15 | EM* AS 225 |
| 2540033050335558784 | 69.64289254 | 46.07931533 | HerbigStar | 4.1 | $2426^{+179}_{-171}$ | 15,155 | -3.51 | -86.9 | -0.18 | 2MASS J04383428+4604454 |
| 5308850371274904192 | 144.6439615 | -54.33735311 | HerbigStar | 4.9 | $4127^{+43}_{-168}$ | 19,030 | -5.53 | -135.05 | -0.22 | WRAY 15-413 |
| 4256260466614300928 | 277.3570387 | -6.077050094 | HerbigStar | 3.4 | $2356^{+2}_{-2}$ | 23,218 | -4.82 | -118.08 | -0.24 | EM* MWC 300 |
| 5972325576126499200 | 258.5750060 | -38.98323981 | HerbigStar | 4.9 | $1606^{+154}_{-58}$ | 36,489 | -5.34 | -130.45 | -0.29 | EM* AS 222 |
| 5244283842139776 0 | 12.52486253 | 64.75973916 | HerbigStar | 3.3 | $2013^{+125}_{-125}$ | 17,637 | -2.87 | -71.7 | -0.3 | EM* GGA 2 |
| 5966221298030125056 | 254.7781823 | -42.70234756 | HerbigStar | 4.7 | $956^{+53}_{-19}$ | 36,985 | -7.46 | -180.88 | -0.31 | CD-42 11721 |
| 2200793847233509760 | 340.6742594 | 60.40017141 | HerbigStar | 4.4 | $2621^{+17}_{-22}$ | 35,427 | -5.97 | -145.49 | -0.36 | EM* MWC 657 |
| 4478088939017621 76 | 50.16453913 | 56.39948587 | HerbigStar | 5.4 | $2354^{+87}_{-77}$ | 20,563 | -5.58 | -136.33 | -0.37 | IRAS 03168+5613 |
| 2207583404553554944 | 349.3996767 | 63.75176856 | HerbigStar | 6.0 | $4080^{+342}_{-642}$ | 36,022 | -6.08 | -148.11 | -0.38 | IRAS 23154+6328 |
| 2200017424528999936 | 335.8737099 | 57.63028127 | HerbigStar | 3.9 | $6590^{+767}_{-294}$ | 28,414 | -4.36 | -107.15 | -0.54 | IRAS 22216+5722 |
| 4651696391895922688 | 81.94851316 | -71.81464394 | HerbigStar | 1.5 | $18259^{+1067}_{-234}$ | 36,649 | -6.25 | -152.25 | -0.69 | LHA 120-S 165 |
| 2017612358184192768 | 359.8332589 | 66.38672132 | HerbigStar | 5.2 | $732^{+9}_{-9}$ | 15,027 | -2.88 | -72.05 | -0.77 | [B62] 4 |
| 4663539300349528192 | 78.33864859 | -65.65405506 | HerbigStar | 1.2 | $18123^{+784}_{-653}$ | 24,524 | -4.49 | -110.33 | -0.77 | SSTISAGEMC J051321.26-653914.6 |
| 4060048532745844688 | 271.4125813 | -24.51107999 | HerbigStar | 4.1 | $1365^{+48}_{-48}$ | 15,047 | -4.02 | -99.09 | -0.91 | EM* LkHA 117 |
| 4688847309225362944 | 10.27822154 | -73.35296519 | HerbigStar | 0.6 | $19798^{+238}_{-36}$ | 19,658 | -2.25 | -57.08 | -0.93 | OGLE SMC-SC2 61751 |
| 5338335905897507456 | 163.5428339 | -60.08733453 | HerbigStar | 2.5 | $8086^{+222}_{-143}$ | 15,007 | -5.82 | -142.0 | -0.99 | 2MASS J10541029-6005145 |
| 4661559629674731776 | 74.40327132 | -67.79371587 | HerbigStar | 1.5 | $10414^{+410}_{-206}$ | 32,534 | -7.78 | -188.65 | -1.01 | LHA 120-S 12 |
| 5615056663019267584 | 114.7756575 | -24.75136361 | HerbigStar | 2.5 | $3116^{+139}_{-393}$ | 40,742 | -6.03 | -146.95 | -1.13 | CD-24 5721 |
| 2015202228869842080 | 347.8139981 | 62.45698608 | HerbigStar | 4.7 | $2277^{+108}_{-52}$ | 15,013 | -2.7 | -67.71 | -1.13 | HBHA 6207-19 |
| 4651968177420876160 | 78.0377423 | -71.11381847 | HerbigStar | 1.2 | $15904^{+497}_{-78}$ | 16,345 | -2.42 | -61.16 | -1.24 | LHA 120-S 160 |
| 3344973478481675264 | 94.68967401 | 15.28117676 | HerbigStar | 4.3 | $2317^{+312}_{-47}$ | 35,001 | -10.69 | -257.9 | -1.38 | EM* MWC 137 |
| 4654808699979503744 | 71.48072022 | -70.84493333 | HerbigStar | 2.7 | $15829^{+40}_{-39}$ | 30,005 | -7.88 | -190.97 | -1.45 | UCAC2 1445227 |
| 4655158131209278464 | 74.19618924 | -69.84021409 | HerbigStar | 1.3 | $10738^{+149}_{-130}$ | 20,610 | -2.53 | -63.77 | -1.66 | HD 268835 |
| 2006219223007452032 | 334.5353473 | 56.09809927 | HerbigStar | 3.5 | $6064^{+633}_{-525}$ | 28,955 | -4.25 | -104.53 | -0.12 | Not listed in SIMBAD |
| 5869126656055392000 | 202.9565261 | -60.39146338 | HerbigStar | 4.6 | $5041^{+657}_{-198}$ | 15,019 | -3.13 | -78.0 | -0.25 | Not listed in SIMBAD |
| 5863990940342000000 | 201.7669711 | -65.3231748 | HerbigStar | 3.0 | $6916^{+557}_{-557}$ | 15,236 | -3.19 | -79.38 | -0.26 | Not listed in SIMBAD |
| 5308151081881494144 | 147.5873831 | -55.01594503 | HerbigStar | 4.7 | $4934^{+992}_{-914}$ | 16,104 | -2.8 | -70.06 | -0.49 | Not listed in SIMBAD |
| 5978823075745899520 | 258.3254263 | -34.52832928 | HerbigStar | 3.7 | $8391^{+971}_{-935}$ | 15,005 | -3.23 | -80.25 | -1.37 | Not listed in SIMBAD |
| 4090887629972125056 | 273.9313886 | -21.63773383 | HerbigStar | 3.6 | $5762^{+82}_{-586}$ | 31,272 | -6.65 | -161.73 | -1.4 | Not listed in SIMBAD |
| 5308789863772681728 | 145.2286581 | -54.59275441 | HerbigStar | 5.2 | $3065^{+249}_{-344}$ | 15,021 | -2.83 | -70.87 | -1.55 | Not listed in SIMBAD |
| 2169119540626866976 | 313.7419439 | 47.76434051 | HerbigStar | 3.8 | $5482^{+390}_{-1715}$ | 15,587 | -2.43 | -61.34 | -1.72 | Not listed in SIMBAD |

## Appendix B: Table containing the details of early HBe stars studied in this work

**Table B.1.** Table of early HBe stars studied in this work along with the basic parameters such as the spectral type, mass, and A$_V$ from Guzmán-Díaz et al. (2021); the EW of H$\alpha$ from Vioque et al. (2018); and the assigned type (intense and weak) of HBe from this work. The $n$(J−H) Lada index was calculated using 2MASS photmetric magnitudes.

| Object Name | Spectral Type | Mass ($M_\odot$) | Av (mag) | EWHa (Å) | $n$(J-H) | Class |
|---|---|---|---|---|---|---|
| CPM 25 | B3-B4 | $6.78^{+1.05}_{-1.18}$ | $4.5 \pm 0.1$ | -200.20 | 0.243 | Intense_HBe |
| HD 200775 | B4 | $7.01^{+0.09}_{-0.01}$ | $2.0 \pm 0$ | -63.83 | -1.015 | Intense_HBe |
| HD 323771 | B5-B6 | $4.22^{+0.16}_{-0.62}$ | $1.5 \pm 0.19$ | -59.35 | 0.234 | Intense_HBe |
| HD 87643 | B4 | $16.02^{+3.98}_{-5.23}$ | $2.5 \pm 0.17$ | -145.20 | 1.397 | Intense_HBe |
| Hen 3-1121 | B1-B2 | $10.99^{+1.09}_{-1.95}$ | $4.0 \pm 0$ | -135.41 | 0.215 | Intense_HBe |
| Hen 3-938 | O | $43.92^{+2.33}_{-3.99}$ | $5.5 \pm 0$ | -92.95 | 0.749 | Intense_HBe |
| MWC 1080 | B0 | $17.97^{+1.91}_{-2.03}$ | $5.0 \pm 0.19$ | -113.19 | 0.571 | Intense_HBe |
| MWC 878 | B0 | $18.05^{+1.17}_{-0.34}$ | $3.5 \pm 0$ | -55.19 | -1.151 | Intense_HBe |
| PDS 27 | B4-B5 | $11.65^{+1.09}_{-1.6}$ | $5.0 \pm 0.07$ | -77.6 | 0.545 | Intense_HBe |
| PDS 34 | B4 | $4.31^{+0.29}_{-0}$ | $3.0 \pm 0$ | -50.20 | 0.110 | Intense_HBe |
| PDS 37 | B2-B3 | $9.04^{+0.73}_{-0.21}$ | $5.5 \pm 0$ | -123.76 | 1.588 | Intense_HBe |
| PDS 477 | B2-B3 | $12.17^{+3.18}_{-3.74}$ | $4.5 \pm 0$ | -121.19 | 0.596 | Intense_HBe |
| PDS 581 | B2-B3 | $7.85^{+0.39}_{-0.85}$ | $3.0 \pm 0$ | -201.19 | 2.86 | Intense_HBe |
| V431 Sct | B2 | $11.21^{+0.68}_{-0.21}$ | $4.0 \pm 0$ | -126.20 | -0.124 | Intense_HBe |
| V921 Sco | B0-B1 | $23.47^{+1.11}_{-3.45}$ | $5.5 \pm 0$ | -195.49 | -0.128 | Intense_HBe |
| HBC 7 | B2-B3 | $8.79^{+0.21}_{-0.57}$ | $4.5 \pm 0$ | -41.81 | -2.588 | Weak_HBe |
| HBC 705 | B2 | $9.28^{+0.69}_{-0.3}$ | $5.5 \pm 0$ | -27.11 | -2.509 | Weak_HBe |
| HD 141926 | B0 | $16.91^{+1}_{-0.88}$ | $2.5 \pm 0.09$ | -46.88 | -2.429 | Weak_HBe |
| HD 305298 | O | $23.22^{+1.03}_{-2.94}$ | $2.0 \pm 0.18$ | -3.24 | -2.687 | Weak_HBe |
| HD 313571 | B4 | $9.54^{+0.46}_{-0.54}$ | $2.5 \pm 0$ | -38.83 | -2.359 | Weak_HBe |
| HD 50083 | B3-B4 | $12^{+0.43}_{-0.56}$ | $1.0 \pm 0$ | -47.83 | -2.445 | Weak_HBe |
| HD 76534 | B2 | $8.61^{+0.37}_{-0.54}$ | $1.0 \pm 0$ | -16.84 | -2.839 | Weak_HBe |
| Hen 3-1121S | O-B0 | $19.14^{+3.92}_{-3.44}$ | $3.5 \pm 0$ | -1.29 | -3.100 | Weak_HBe |
| Hen 3-823 | B4 | $6.28^{+0.68}_{-0.65}$ | $1.5 \pm 0$ | -29.83 | -2.525 | Weak_HBe |
| IL Cep | B2 | $10.02^{+0.1}_{-0.02}$ | $3.0 \pm 0$ | -22.83 | -2.617 | Weak_HBe |
| MWC 655 | B2-B3 | $11^{+0.52}_{-0.37}$ | $1.5 \pm 0.07$ | -15.49 | -2.267 | Weak_HBe |
| MWC 953 | B4 | $12.06^{+1.88}_{-1.22}$ | $3.5 \pm 0.14$ | -32.21 | -2.273 | Weak_HBe |
| PDS 286 | B0 | $26.08^{+1.41}_{-1.55}$ | $6.0 \pm 0$ | -30.77 | -2.566 | Weak_HBe |
| PDS 344 | B5-B6 | $3.56^{+0.24}_{-0}$ | $1.5 \pm 0$ | -30.03 | -2.156 | Weak_HBe |
| PDS 361S | B3-B4 | $5.85^{+0.16}_{-0.07}$ | $2.0 \pm 0$ | -9.32 | -2.394 | Weak_HBe |
| PDS 543 | O-B0 | $26.92^{+1.07}_{-2.44}$ | $6.5 \pm 0$ | -2.19 | -3.13 | Weak_HBe |
| V361 Cep | B4 | $5.54^{+0.06}_{-0.11}$ | $2.0 \pm 0$ | -32.59 | -2.293 | Weak_HBe |
| WRAY 15-1435 | B2-B3 | $9.69^{+0.31}_{-0.63}$ | $4.0 \pm 0$ | -21.19 | -2.089 | Weak_HBe |